Supplementary materials for

Towards understanding the origin of massive dolostones

Meng Ning[a], Xianguo Lang[b,] Kangjun Huang[c], Chao Li[d], Tianzheng Huang[a], Honglin Yuan[c], Chaochao Xing[a], Runyu Yang[a], and Bing Shen[a1]

[a]Key Laboratory of Orogenic Belts and Crustal Evolution, MOE, School of Earth and Space Sciences, Peking University, Beijing, China;

[b]State Key Laboratory of Oil and Gas Reservoir Geology and Exploitation & Institute of Sedimentary Geology, Chengdu University of Technology, Chengdu, China;

[c]State Key Laboratory of Continental Dynamics and Shannxi Key Laboratory of Early Life and Environment, Department of Geology, Northwest University, Xi'an, China;

[d]National Research Center for Geoanalysis, Chinese Academy of Geological Sciences, Beijing, China

[1]Corresponding author: Bing Shen (bingshen@pku.edu.cn)

This PDF file includes:

Supplementary text

Figures S1 to S4

Tables S1 to S3

References for Supplementary materials citations

Supplementary Text

Sedimentological and stratigraphic context

During middle to late Cambrian, the Yangtze Platform inheritably developed as a shallow water carbonate platform (Feng et al., 2001), allowing the formation of massive dolostone succession, which wedging out from northwest to southeast in South China and representing the progradation process associated with relative sea level falling (Mei, 2007). The middle Cambrian Qinjiamiao (QJM) Formation in studied area is stratigraphically divided into 4 members with a total thickness of 300 m (Fig. S1). The first member mainly consists of 100-m-thick dolostone, followed by 5~10-m-thick feldspar quartz sandstone (second member). The rest can be subdivided into, in stratigraphic order, about 80-m-thick dolostone with stromatolites of the third member, and 120-m-thick dolostone (fourth member).

The focus of this study is a 3.2 m stratigraphic interval of the first member of the QJM Formation. In general, the lower to middle part of the section is dominated by gray thin-middle bedded dolostone (Fig. S2), interbedded with middle bedded sandy ooid dolostone (Fig. S2E) and laminated dolomicrite (Fig. S2D). Some layers contain quartz sands flaser beds (see Fig. S2C for details). The top part consists of grey to yellow thin bedded muddy dolostone (Fig. S2B) with siliciclasts and pseudomorphs of gypsum (Fig. S2a).

Lithofacies analysis

Facies analysis integrated observations from outcrop, hand specimens, and thin sections to document lithology, rock fabric, sedimentary structures, and stratigraphic surfaces. The QJM Formation exposed in the studied section consists of 8 facies:

L1- Dolomitized mudstone with pseudomorphs of gypsum. This lithofacies is mainly composed of dolomicrite. This facies contains lath-shaped gypsum pseudomorphs and has no subaerial exposure features. This facies association can be interpreted as a supratidal salina pond deposit.

L2- Laminated argillaceous dolomitized mudstone. Composed of dolomicrite, organic matter and rare fine-grained quartz sand with microspar calcite filling the fenestrate structures and burrows. These deposits can be distinguishable from L1 lithofacies with the lack of evaporites, indicating a

supratidal flat environment.

L3- Mixed siliciclastic-dolomicrite. Siliciclasts interbed with dolomicrite. It is common to develop flaser and wavy bedding in this kind of lithofacies (Fig. S2C and E). The siliciclasts layers were probably deposited during the advance of siliciclastics into the coastal plain area during periods of continental flooding. Eolian quartz sand from terrestrial sources could also add considerable sediment to the arid tidal flat system such as those in the Arabian Gulf (Shinn, 1973).

L4- Micro-crystalline dolomite with remanent algae fabric. Composed of micro-crystalline dolomite with remanent algae fabric. Recognition of the original algae fabrics here is the abundance of dense, micritic masses (dark material) that may have formed by decomposition of primary material.

L5- Medium-crystalline dolomite with fabric destructed. Subhedral medium-crystalline dolomites are tightly packed with the development of straight, compromise boundaries, resulting in complete obliteration of primary fabrics.

L6- Dolomitized peloid packstone. Composed of dolomitized peloid and fine-grained quartz sand. Note the poor sorting and distinct differences in size and shape of peloids, which indicate that these grains originated from the reworking of weakly lithified carbonate mud and cemented by crystalline dolomite.

L7- Quartzose ooid grainstone. This lithofacies contains abundant dolomitized ooids and well sorted very fine- to fine-grained quartz sand (Fig. S3). Peloids can serve as nuclei for ooids. Some ooids exhibiting primary concentric fabrics may indicate dolomitization subsequent to an aragonite or high-Mg calcite stage. There are sharp surfaces between the submarine-cemented hardground and overlying oolitic or peloid sediments in L6 and L7. These lithified sediments can form intraclasts which can subsequently be transported as sedimentary particles again from erosion and transport of semi- consolidated muds.

L8- Intraclast dominated dolomicrite packstone to grainstone. These grains are mm- to cm-sized irregularly-shaped, predominantly micritic clasts and cemented by crystalline dolomite, which represents rip-up clasts. The clasts can be interpreted as a result of early lithification of carbonate mud, followed by exhumation of the lithified parts by weak currents, erosion and encrustation at the surface, redeposition within the mud and additional continued accretionary growth in the sediment. These incipient tidal intraclasts are abundant in the upper part of subtidal zones where scouring

undermines lithified mud beds (Flügel, 2010).

Sedimentary environment and shallowing-upward cycles

Facies associations and petrological evidences suggest an evaporitic seasonal river-influenced, mixed carbonate-siliciclastic tidal flat depositional systems of the QJM Formation (Fig. S2). Similar sedimentary environments are found in many other Cambrian successions (Lasemi et al., 2012; Spencer and Demicco, 1993; Zand-Moghadam et al., 2013). The most diagnostic sedimentary structures in the studied tidalites are dominated by tidal bedding (Fig. S2C and E), pseudomorphs of gypsum (Fig. S2a), and fenestrate structures (Fig. S3B). The supratidal is characterized by laminated dolomicrite with pseudomorphs of gypsum crystals and fenestrate structures. The intertidal is characterized by thin bedded dolomicrite with remanent algae fabric. The subtidal facies are interlayered with various erosive-based, graded intraclastic storm deposition, including ooids, peloids and intraclasts (Fig. S3).

Seven shallowing-upward sedimentary cycles were recognized in the QJM Formation, while each cycle is bounded by an abrupt change in the inferred depositional environment between the facies above and below the contact, and which represents a subaerial-exposure surface or its correlative conformity. Within a single shallowing-upward cycle, facies boundaries are transitional. Cycle 1 is composed of L6-L4-L2 lithofacies stratigraphically, indicating intertidal to supratidal environment. Cycle 2 consists L8-L4-L2 lithofacies and cycle 3 includs L7-L4-L2 lithofacies, and both of them can be interpreted as complete cycle from subtidal to supratidal environment. Cycle 4 consists L4-L3 lithofacies and cycle 5 consists L5-L1 lithofacies, which represent intertidal to supratidal environment. Cycle 6 is composed of L4-L3-L2-L1 lithofacies and cycle 7 consists L3-L2-L1 lithofacies, which represent shallower intertidal to supratidal environment than Cycle 4 and 5. The observed facies stacking pattern could be ascribed to rapid submergence followed by gradual shallowing of relative sea level.

Rayleigh fractionation model

In the Rayleigh fractionation model, Mg isotopic composition of the remaining seawater ($\delta^{26}Mg_r$) can be expressed as:

$$\delta^{26}\mathrm{Mg_r} = \delta^{26}\mathrm{Mg_0} + 1000 \cdot \mathrm{Z}_{24}^{26} \cdot \ln(\mathrm{F}) \quad \text{(S1)}$$

where $\delta^{26}Mg_0$ is the initial $\delta^{26}Mg$ of original seawater; F is the fraction of remaining Mg; Z is difference of Rayleigh fractionation coefficient between ^{26}Mg and ^{24}Mg. $\delta^{26}Mg_{dol}$ can be calculated by the following equation:

$$\delta^{26}Mg_{dol}=\delta^{26}Mg_r-\Delta_{dol} \quad (S2)$$

where Δ_{dol} is the isotopic fractionation during dolomite formation. When seawater dolomitization in a restricted basin, the vertical profile of $\delta^{26}Mg_{dol}$ reflects the evolution of $\delta^{26}Mg_{df}$ through time.

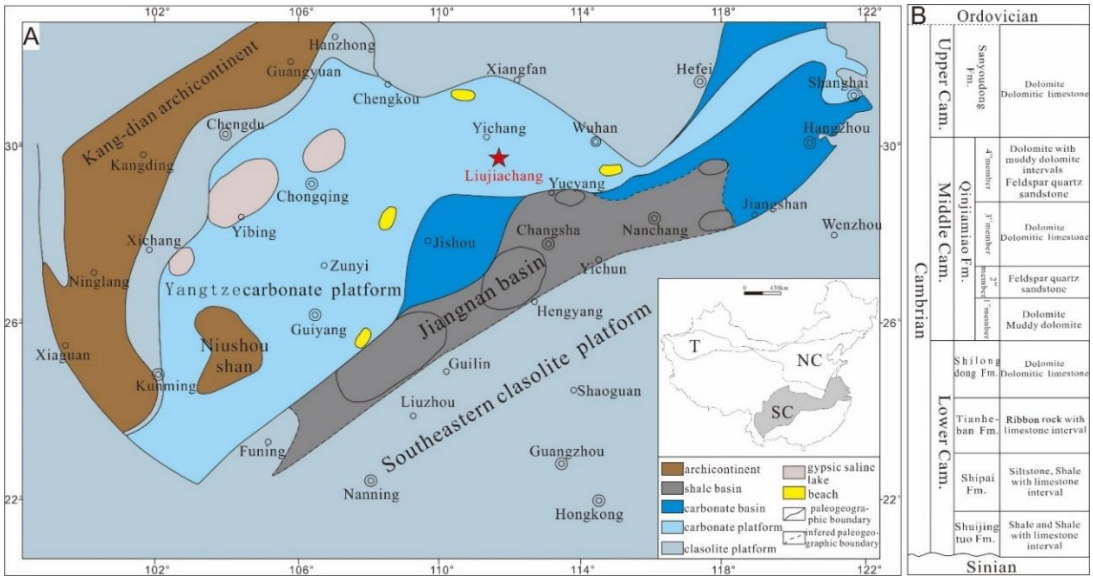

Fig. S1. (A) Middle Cambrian paleogeographic map of the South China Block showing the sampling location (red star) of the Liujiachang section in Hubei province (according to Feng et al. (2001)). (B) Stratigraphic column of the Cambrian succession in South China.

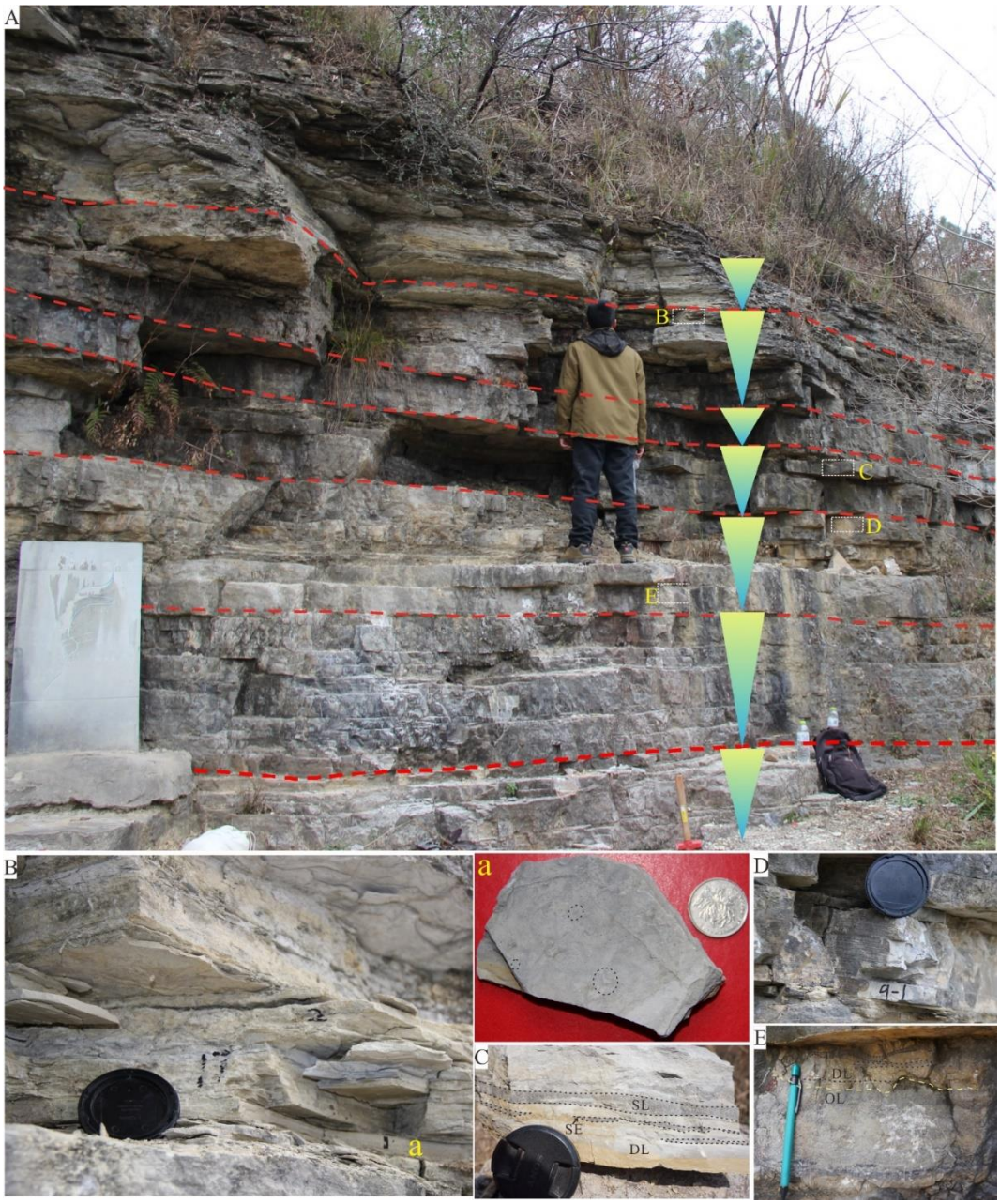

Fig. S2. Stratigraphic outcrop photographs (A) of the Qinjiamiao Formation in the Liujiachang section. Figure A showing 7 shallowing upwards sedimentary cycles. Figures B-E are details of the focus areas in figure B showing typical sedimentary structures. (B)Thin bedded muddy dolostone with pseudomorphs of gypsum, See (a) for the enlarged details. (C) Internal structures of the peritidal deposits. Accumulation of small rippled beds produce lenticular and wavy bedding known as flaser bedding, presenting as a thin sand (quarts) layer (SL) sandwiched by thick dolomicrite layers (DL) with a few thin sand lenses (SE). It is reasonably linked with the formation of rippled laminae, lenticular by waves or combined wave and tide flows instead of purely tides (usually known as tidal bedding), and sandier laminae represents higher energy events of larger waves or the combined flows of larger waves and higher tides instead of purely higher tides. (D) Laminated tidal flat deposits and (E) Field photograph of a succession composed of bluish gray shallow subtidal ooid grainstone (OL) overlain by light yellow intertidal dolomicrite (DL) with flaser-wavy bedding showing as ooid lenses and thin ooid layers. The dashed yellow line indicating an erosional contact.

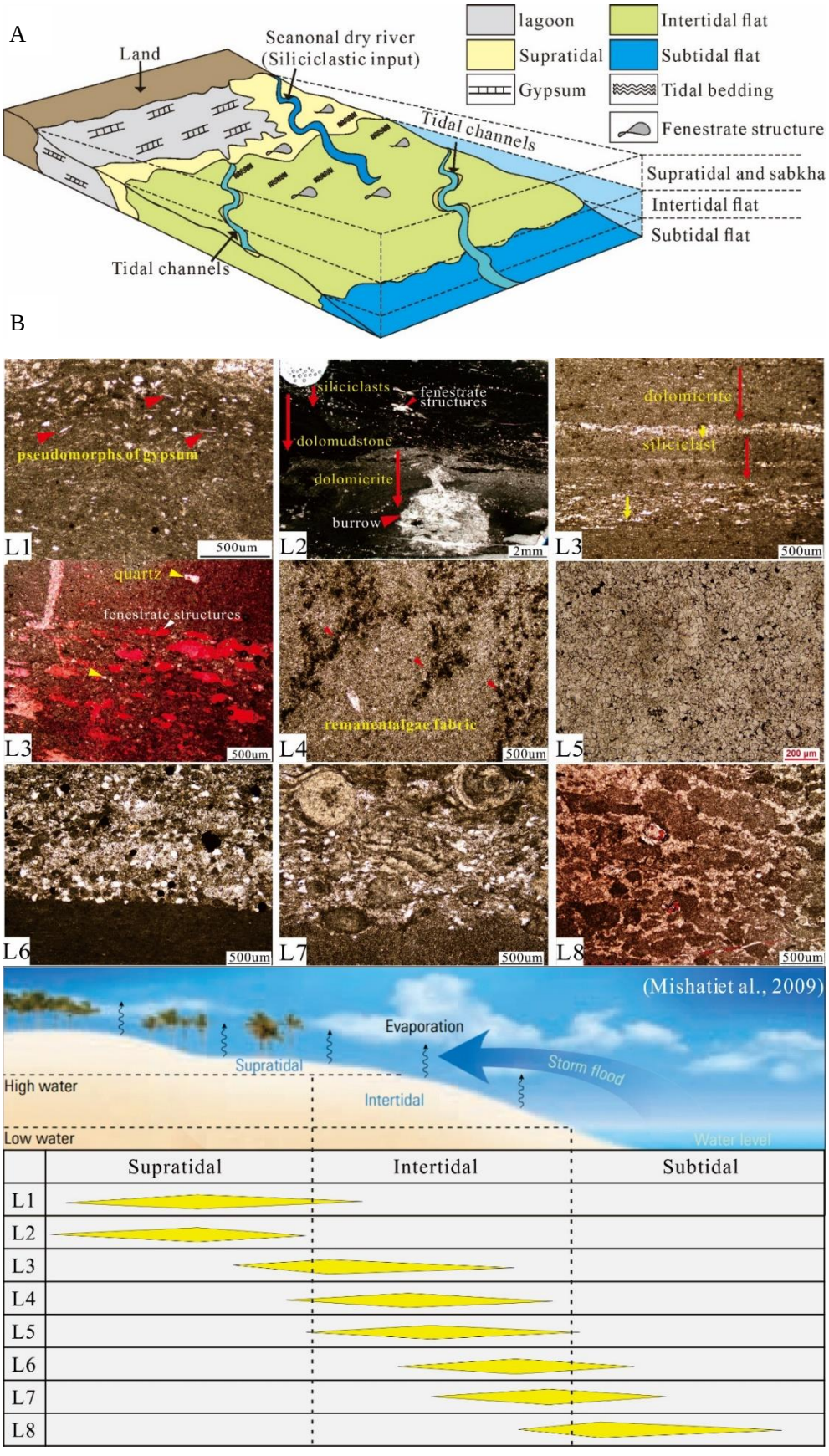

Fig. S3. (A) Depositional model of mixed siliciclastic carbonate tidal flat. microerosive surface. (B) Thin-section photomicrographs of the representative microfacies of the Qinjiamiao Formation.

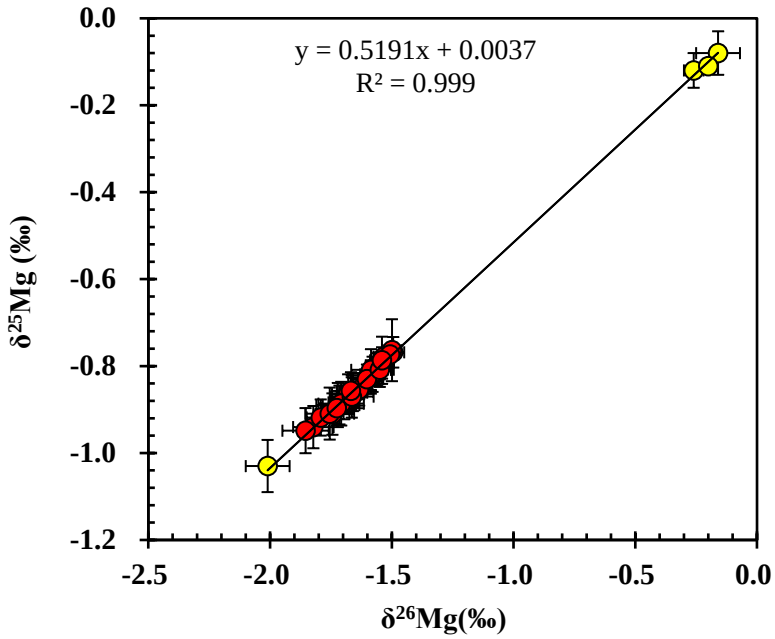

Fig. S4. Crossplot of $\delta^{26}Mg$ and $\delta^{25}Mg$ data of the Qinjiamiao Formation (red marks) and standards (yellow marks).

Table S1. The comparison of modern and ancient dolostones

	Modern dolostone	Ancient dolostone
Distribution	limited geographic distribution eg. sabkha flats, hypersaline lagoons and playa lakes	Extensive (hundreds to thousands of square kilometers)
Thickness	Discrete layers of cm to m	Hundreds to thousands of meters in thickness
Degree of order	Low, non-stoichiometric	High, stoichiometric

Table S2. Microfacies classification, sedimentological and depositional environment interpretation.

Code	Microfacies	Texture	Components	Structures	Depositional environment
L1	Dolomitized mudstone with pseudomorphs of gypsum	M	Dolomicrite	Pseudomorphs of gypsum	Evaporated supratidal
L2	Laminated argillaceous dolomitized mudstone	M	Dolomicrite, microspar calcite filling the fenestrate structures	fenestrate structures, burrows	Supratidal
L3	Mixed siliciclastic-dolomicrite	M-W	Very fine- to fine-grained quartz sand, dolomicrite matrix supported	flaser-wavy bedding fenestrate structures	Intertidal to supratidal
L4	Micro-crystalline dolomite with remanent algae fabric	P	Micro-crystalline dolomite	Remnant algae fabric	Intertidal
L5	Medium-crystalline dolomite with fabric destructed	P-G	Medium crystalline euhedral to subhedral dolomite	fabric destructed	-
L6	Dolomitized peloid packstone	P	Peloids with dolomitized crust	Submarine hardground	Subtidal to intertidal
L7	Quartzose ooid grainstone	G	Dolomitized ooids, quartz grains, dolomicrite cements	Lenticular bedding, Submarine hardgrounds	Subtidal
L8	Intraclast dominated dolomicrite packstone to grainstone	P-G	Rip-up intraclasts, crystalline dolomite cements, fine-grained quartz sand	Rip-up structures	Subtidal

Notes: M-mudstone; W-wackestone; P-packstone; G-grainstone.

Table S3. Mg/Ca ratios and Mg isotopes of standards and dolostone samples from the Qinjiamiao Formation.

Cycle	Sample No.	Mg/Ca (mol/mol)	δ^{26}Mg (‰)	2SD	δ^{25}Mg (‰)	2SD
1	LJC1	1.01	-1.64	0.04	-0.86	0.04
	LJC2	0.96	-1.59	0.04	-0.82	0.03
	LJC3	0.93	-1.59	0.03	-0.83	0.04
	LJC4	0.93	-1.74	0.07	-0.91	0.05
	LJC5	0.98	-1.72	0.09	-0.89	0.05
2	LJC6	0.97	-1.72	0.07	-0.89	0.04
	LJC7	0.95	-1.82	0.08	-0.94	0.05
	LJC8	0.94	-1.68	0.04	-0.87	0.03
	LJC9	0.99	-1.79	0.06	-0.92	0.04
	LJC9-D	0.99	-1.73	0.06	-0.90	0.04
3	LJC10	0.55	-1.66	0.04	-0.86	0.03
	LJC11	0.79	-1.66	0.05	-0.86	0.04
	LJC11-D	0.79	-1.67	0.06	-0.86	0.04
	LJC12	1.01	-1.68	0.07	-0.86	0.05
4	LJC13	1.03	-1.58	0.05	-0.82	0.04
	LJC13-R	1.03	-1.51	0.03	-0.77	0.01
	LJC14	1.02	-1.75	0.10	-0.91	0.06
	LJC15	0.96	-1.70	0.06	-0.88	0.04
	LJC16	1.00	-1.85	0.10	-0.95	0.05
5	LJC17	0.91	-1.49	0.05	-0.77	0.04
	LJC18	0.92	-1.56	0.05	-0.81	0.04
	LJC19	1.00	-1.71	0.09	-0.89	0.05
6	LJC20	0.95	-1.66	0.06	-0.86	0.03
	LJC21	0.99	-1.63	0.03	-0.85	0.04
	LJC22	1.05	-1.53	0.04	-0.78	0.01
	LJC23	1.04	-1.57	0.01	-0.81	0.03
	LJC24	0.98	-1.54	0.05	-0.79	0.04
	LJC25	0.95	-1.50	0.04	-0.76	0.07
7	LJC26	0.97	-1.66	0.09	-0.87	0.05
	LJC27	0.81	-1.59	0.08	-0.81	0.05
	LJC27-R	0.81	-1.54	0.05	-0.79	0.05
	LJC28	0.95	-1.60	0.07	-0.83	0.03
	LJC29	0.57	-1.55	0.06	-0.81	0.04
Standard	BCR-2-1	-	-0.16	0.09	-0.08	0.05
	BHVO-2-1	-	-0.26	0.04	-0.12	0.04
	BHVO-2-2	-	-0.20	0.02	-0.11	0.01
	Ca:Mg-4	-	-2.01	0.09	-1.03	0.06
Recommended value	BCR-2	-	-0.22	0.06	-0.10	0.02
	BHVO-2	-	-0.24	0.08	-0.12	0.05
	GSB-pure Mg	-	-2.02	0.03	-1.03	0.02

Notes: 2SD = 2 times the standard deviation of the population of n (n>3) repeat measurements of the standards during an analytical session. D-duplicate; R-replicate. GSB-Mg is an ultrapure single elemental standard solution from China Iron and Steel Research Institute.

References

Feng, Z., Peng, Y., Jin, Z., Jiang, P., Bao, Z., Luo, Z., Ju, T., Tian, H., Wang, H., 2001. Lithofacies palaeogeography of the Cambrian in South China. Journal of palaeogeography 3, 1-18.

Flügel, E., 2010. Microfacies of Carbonate Rocks. Springer Berlin Heidelberg.

Lasemi, Y., Jahani, D., Amin-Rasouli, H., Lasemi, Z., 2012. Ancient Carbonate Tidalites, in: Davis Jr, R.A., Dalrymple, R.W. (Eds.), Principles of Tidal Sedimentology. Springer Netherlands, Dordrecht, pp. 567-607.

Mei, M.X., 2007. Sequence stratigraphic framework and its palaeogeographic setting for the Loushanguan Group dolostones of Cambrian in Upper Yangtze Region. Journal of Palaeogeography 9, 117-132.

Shinn, E.A., 1973. Carbonate Coastal Accretion In an Area of long shore Transport ,N.E. Qatar Persian Gulf, in: Purser, B.H. (Ed.), The Persian Gulf Springer Verlag, Berlin, Heidelberg, New York, pp. 179-191.

Spencer, R.J., Demicco, R.V., 1993. Depositional environments of the Middle Cambrian Arctomys Formation, southern Canadian Rocky Mountains. Bulletin of Canadian Petroleum Geology 41, 373-388.

Zand-Moghadam, H., Moussavi-Harami, R., Mahboubi, A., Bavi, H., 2013. Comparison of Tidalites in Siliciclastic, Carbonate, and Mixed Siliciclastic-Carbonate Systems: Examples from Cambrian and Devonian Deposits of East-Central Iran. ISRN Geology 2013, 21.